Atom-Scale Ptychographic Electron Diffractive Imaging of Boron Nitride Cones

Corey T. Putkunz,[1,*] Adrian J. D'Alfonso,[1] Andrew J. Morgan,[1] Matthew Weyland,[2,3] Christian Dwyer,[2,3,4] Laure Bourgeois,[2,3] Joanne Etheridge,[2,3] Ann Roberts,[1] Robert E. Scholten,[1,5] Keith A. Nugent,[1,5] and Leslie J. Allen[1]

[1]*School of Physics, The University of Melbourne, Victoria 3010, Australia*
[2]*Monash Centre for Electron Microscopy, Monash University, Victoria 3800, Australia*
[3]*Department of Materials Engineering, Monash University, Victoria 3800, Australia*
[4]*Australian Research Council Centre of Excellence for Design in Light Metals*
[5]*Australian Research Council Centre of Excellence for Coherent X-Ray Science*

(Received 25 September 2011; published 14 February 2012)

Ptychographic coherent diffractive imaging (CDI) has been extensively applied using both x rays and electrons. The extension to atomic resolution has been elusive. This Letter demonstrates ptychographic electron diffractive imaging at atomic resolution, permitting identification of structure in a boron nitride helical cone at a resolution of order 1 Å, beyond that of comparative *Z*-contrast images. A scanning transmission electron microscope is used to create a diverging illumination in a defocused Fresnel CDI geometry, providing a robust strategy leading to a unique solution.

DOI: 10.1103/PhysRevLett.108.073901 PACS numbers: 42.30.Rx, 42.30.Wb

Elucidating structure at the atomic scale is crucial for the development of modern materials in nanotechnology. Examples of such materials are the allotropes of carbon, including buckminsterfullerenes [1] and graphene [2]. Scanning transmission electron microscopy (STEM) and transmission electron microscopy (TEM) play a key role in structural determination at atomic length scales. As an alternative microscopy technique, diffractive imaging combined with ptychography would provide a valuable complement for studying atomic structure. Ptychographic electron coherent diffractive imaging (PECDI) combines diffraction data recorded using overlapping probe positions. In this Letter we demonstrate PECDI at the atomic scale. We show that, for a given STEM probe, PECDI provides structural information at a resolution greater than that obtained in the corresponding *Z*-contrast images.

In general, CDI recovers the exit wave field of a specimen from far-field diffraction data using various phase retrieval methods [3]. High resolution CDI was first demonstrated using x rays [4], and has since led to many advances in phase retrieval algorithms, geometries for more effective data collection, and methods of coping with partial spatial coherence in the illuminating fields. Under the condition that the recovered transmission function of the specimen is equivalent to a linear integration through its atomic potential, the quantitative nature of CDI will also permit tomography at atomic resolution [5,6].

There have been a number of nonptychographic demonstrations of electron coherent diffraction imaging (ECDI) at atomic resolution, often used in conjunction with TEM images [7,8], or reconstructed *a priori* from diffraction data recorded with a single probe position [9–11]. A major hurdle present in ECDI, particularly when using plane wave illumination, is the large dynamic range required to record both the intense Bragg peaks and the weak scatter that lies between. Failure to measure this weak scatter results in arbitrary relative phase offsets of the Bragg peaks following iterative phase retrieval, leading to a nonunique solution. Illuminating the specimen with a STEM probe focused before the specimen creates convergent beam electron diffraction (CBED) disks in the far field. Adjustments can be made until the point where the CBED disks overlap, ensuring no isolated regions exist in the diffraction data. The large defocus distances present in this Fresnel CDI geometry also impart strong phase curvature across the illuminating beam [12–14], enhancing the ability of iterative phase retrieval algorithms to arrive at a unique solution [15].

Recent advances in diffractive imaging utilize a probe scanned across a specimen in a geometry which results in each element of interest being illuminated multiple times from a different region of the probe (different in amplitude or phase), imparting diversity in the diffraction data. Ptychography was originally proposed as a method of overcoming resolution limits in electron microscopy [16,17]. When applied to CDI, ptychography [18] provides significant improvements in reconstruction quality by reducing erroneous pathways that iterative algorithms can take as they traverse solution space. This results in far fewer artifacts in the recovered images and the ability to image extended objects. Ptychographic methods which also incorporate iterative probe retrieval into the image reconstructions show further improvements in reconstruction quality [19]. While PECDI has been performed at relatively low resolution [20], to date these methods have yet to be applied at resolutions which allow atomic structure to be observed.

The specimen investigated was a cone-shaped particle consisting of a helically wound boron nitride (BN) layer, as shown in the large field of view annular dark-field (ADF)

STEM image in Fig. 1(a). The conical morphology arises from a topological defect in the BN hexagonal lattice. Such structures are of interest due to their potential applications as field emitters and mechanical springs [21].

The BN cone was placed on a holey carbon film, such that the regions of interest protruded into a void in the film. This ameliorates diffuse scattering from the support film. Electron diffraction data were recorded using an FEI Titan^3 80–300 microscope, installed in an ultrastable environment, operating at an electron energy of 300 keV corresponding to a wavelength of 2 pm. For the detailed examination of the regions of interest shown as white boxes in Fig. 1(a) the STEM illumination for PECDI was created using a probe-forming aperture with a convergence semiangle of 10 mrad. Comparative ADF images of the specimen were also recorded using this probe focused at the specimen plane. To record PECDI data the probe was focused such that the BN sample was 160 nm beyond the focus of the probe, producing an illumination in a Fresnel CDI geometry [12] with significant phase curvature across the diameter of the illumination (Fresnel number $N_F = 9$) [15]. In this overfocused geometry the diameter of the probe was 32 Å in the plane of the specimen. The electron current was 63 pA, or 3.9×10^8 e^-/s, and for a single exposure the electron fluence incident on the sample was 4.6×10^5 $e^-/\text{Å}^2$. The probe was scanned across each of two regions on the BN sample in a 5×4 grid using 10 Å steps to facilitate the ptychography requirements of a significant overlap between adjacent probe positions.

At each probe position diffraction data were recorded with a 1 s exposure, an example of which is shown in Fig. 1(b). The detector used was a Gatan UltraScan™ 1000, which had a numerical resolution of 1.3 Å^{-1} in this geometry. Data were also recorded with the probe passing through a void in the carbon film. This provided an accurate starting guess of the probe amplitude for the iterative algorithm. Recording the probe data in the vicinity of the specimen, rather than with the specimen completely removed, incorporated the effects of specimen surface charge into the measured probe. Exposures of equal length with no electrons were recorded to correct for detector noise. Further insight into the illuminating wave field was provided by the CEOS Cs aberration correction software [22].

PECDI generally requires explicit knowledge of the probe, as it must be separated from the object function many times during an iterative reconstruction. In the ideal case the exit wave field of the specimen for the jth probe position ψ_j is related to the object transmission function T via

$$\psi_j(\boldsymbol{\rho}_s) = \psi_0(\boldsymbol{\rho}_s - \boldsymbol{\rho}_j)T(\boldsymbol{\rho}_s), \quad (1)$$

where $\boldsymbol{\rho}_s$ is the 2D real space coordinate, ψ_0 is the incident probe, and $\boldsymbol{\rho}_j$ is the ptychographic offset. Situations where Eq. (1) does not hold inhibits the use of ptychographic

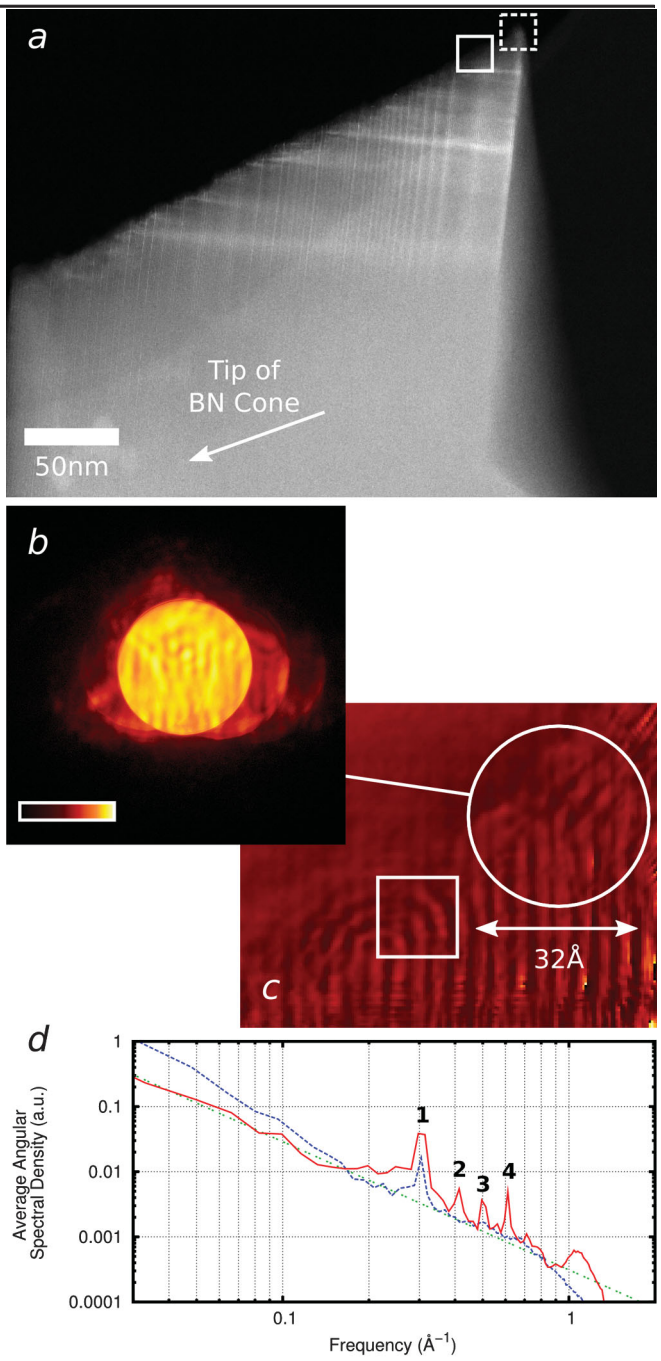

FIG. 1 (color). (a) Large ADF image of the BN cone showing the region of interest imaged in (c) as a small solid white box. Also depicted is the direction of the tip of the BN cone. (b) Sample diffraction data (on a logarithmic intensity scale) for a single probe position, shown to scale as a 32 Å white circle in (c). (c) PECDI image of the edge of the BN cone. Color map represents the phase of the reconstructed transmission function. The white box highlights the reconstruction of in-plane (100) columns. (d) Averaged radial power spectral density (PSD) as a function of spatial frequency for the PECDI reconstruction (red solid line) and an ADF image of the same region (blue dashed line). The peaks labeled 1–4 are discussed in the main text. The green dotted line represents a power law fit with a slope of −2.0. Significant deviation of the PECDI PSD occurs at a spatial frequency of approximately $q = 1.0$ Å^{-1}.

methods to date. However, advances which allow multislice methods to be incorporated into PECDI may extend the validity of the approach [23]. Imaging thin regions of a specimen containing light elements such as boron and nitrogen in the absence of any membrane or support film ensures Eq. (1) is satisfied here, as confirmed by the subsequent analysis.

In conjunction with ptychography, those diffractive imaging methods which enable *in situ* probe retrieval offer the most promising solution for performing PECDI. For this study a variation of the method of scanning x-ray diffraction microscopy (SXDM) was used, described in detail by Thibault *et al.* [19]. The SXDM algorithm decouples Eq. (1) to solve for both the probe and the object transmission function, recalculating each in turn at the beginning of every iteration. The modified SXDM algorithm then uses Eq. (1) as a constraint to the solution in real space, along with the typical Fourier constraint in reciprocal space, which involves forward propagating the exit wave from each probe position and reapplying the measured intensity to the complex wave field. These two constraints are used in conjunction with both error reduction [24] and the difference map algorithm [25] in turn to provide feedback and stop stagnation during the phase retrieval. While the algorithm optimizes the initial estimate of the probe, an accurate initial guess of the probe wave field proved important in recovering the object transmission function. Accordingly, the measured probe data with the aberration coefficients and the propagator based on the correct focus to specimen distance applied to the phase were used as input for the algorithm. At every fifth iteration the measured far-field probe intensity was applied as a further modulus constraint to the probe.

The PECDI phase retrieval of the regions shown in white boxes in Fig. 1(a) converged to a stable solution in less than 60 iterations, though an interpretable image was provided after approximately 10 iterations, making rapid feedback a possibility. Figure 1(c) shows the PECDI reconstruction of the edge of the BN helical cone. Distinct lattice planes are visible, corresponding to various layers inside the stacked cone. These atomic planes, with a spacing of 3.3 Å, are consistent with the locations of centers of the CBED disks visible in the diffraction data for a single probe position, shown in Fig. 1(b). In the reconstruction it is possible to observe atomic structure not present in an ADF image recorded using the same probe, in the form of in-plane lattice fringes with a spacing of approximately 2 Å in association with BN loops at the edge of the cone [white box in Fig. 1(c)]. These loops correspond to tubular regions where the BN edges join in order to remove their dangling bonds. The in-plane fringes suggest local hexagonal BN stacking in the loops.

Numerous methods exist for determining the final resolution of diffractive imaging results [26,27]. For the BN cone images the resolution was calculated by analyzing the average power spectral density (PSD) of the recovered object function and determining where this function deviates from an ideal power law, into a regime dominated by noise. The PSD corresponding to the reconstruction in Fig. 1(c) is shown in 1(d), demonstrating an imaging resolution of approximately 1.0 $Å^{-1}$, beyond the 0.5 $Å^{-1}$ limit defined by the convergence angle of the probe. Back propagation of the probe recovered during the iterative phase retrieval to its beam waist also gives a measure of the potential STEM resolution, resulting in a FWHM = 1.21 Å, or 20% lower resolution than the PECDI reconstruction. The peaks labeled 1, 2, and 4 in Fig. 1(d) strongly suggest (002), (100), and (004) layers are present, respectively, in the reconstruction, since the corresponding fringes can be identified in (c). The fringes corresponding to peak 3 are harder to identify. The PSD for the same region in the ADF image shows no structure below the (002) fringe and deviates from an ideal power law at approximately 0.8 $Å^{-1}$.

Development of methods for incorporating partial coherence effects into iterative phase retrieval [28,29] were also included in the reconstructions. Here the method of Clark and Peele [29] was used to iteratively refine the coherence length of the probe, which in reciprocal space was calculated to be $l_c = 0.66 \pm 0.3$ $Å^{-1}$, by incorporating this partial spatial coherence into every instance of the modulus constraint. The iteratively refined estimate of l_c agrees with previous coherence measurements for the instrument [30]. We note that results without incorporating these corrections into the reconstructions do not materially affect the results.

The additional contrast provided by PECDI is highlighted in Fig. 2. Figure 2(a) shows a PECDI reconstruction of a separate region of interest on the BN cone, shown as a dashed white box in Fig. 1(a). This region corresponds to the lower corner of the BN cone which was thicker than that imaged in Fig. 1(c), a more severe test of the validity of Eq. (1). A direct comparison of the PECDI and ADF images is shown in (a) and (b), respectively, with the PECDI reconstruction also showing increased sensitivity to weak scattering near the specimen boundary. Higher resolution ADF images were also recorded in Fig. 2(c)

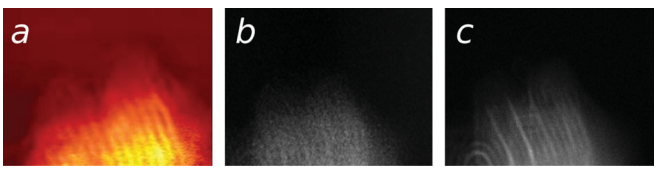

FIG. 2 (color). Comparison of PECDI and ADF images for a region inside the dashed white box in Fig. 1(a). (a) Phase of the transmission function recovered using PECDI. (b) ADF image recorded with the same 10 mrad probe used to create (a), though focused on the specimen. (c) ADF image recorded using a 14 mrad probe.

for verification of features not present in the lower resolution images.

In conclusion, we have demonstrated atomic resolution ptychographic electron diffractive imaging of a helical BN cone. Using a small probe in a diverging geometry (32 Å diameter in the specimen plane), rather than a plane wave or pencil probe, produced continuous diffraction data in the form of overlapping CBED disks in contrast to isolated Bragg spots. This continuous diffraction data led to a unique reconstruction of the object transmission function using ptychographic phase retrieval incorporating the effects of partial spatial coherence. PECDI of the BN cone to a resolution of order 1.0 Å produced images of the terminations of atomic planes. The ability to image regions of interest within extended objects also removes the requirements of an isolated specimen. Furthermore, the sensitivity and quantitative nature of this technique has potential for use with atomic resolution tomography of specimens with light elements such as carbon nanotubes.

The authors express gratitude to Professor Y. Bando (National Institute of Materials Science, Japan) for provision of the BN sample. Experimental work was performed at the Monash Centre for Electron Microscopy, using instrumentation that was supported by the Australian Research Council infrastructure Grant No. LE0454166. This research was supported under Australian Research Council's Discovery Projects funding scheme (Project No. DP1096025).

*Corresponding author.
cputkunz@unimelb.edu.au

[1] H. W. Kroto *et al.*, Nature (London) **318**, 162 (1985).
[2] A. K. Geim and K. S. Novoselov, Nature Mater. **6**, 183 (2007).
[3] R. W. Gerchberg and W. O. Saxton, Optik (Stuttgart) **35**, 237 (1972).
[4] J. Miao, D. Sayre, and H. N. Chapman, J. Opt. Soc. Am. A **15**, 1662 (1998).
[5] C. T. Putkunz *et al.*, Opt. Express **18**, 11746 (2010).
[6] M. Dierolf *et al.*, Nature (London) **467**, 436 (2010).
[7] W. J. Huang *et al.*, Nature Phys. **5**, 129 (2008).
[8] L. De Caro *et al.*, Nature Nanotech. **5**, 360 (2010).
[9] J. M. Zuo *et al.*, Science **300**, 1419 (2003).
[10] R. Dronyak *et al.*, Appl. Phys. Lett. **95**, 111908 (2009).
[11] O. Kamimura *et al.*, Ultramicroscopy **110**, 130 (2010).
[12] G. J. Williams *et al.*, Phys. Rev. Lett. **97**, 025506 (2006).
[13] D. J. Vine *et al.*, Phys. Rev. A **80**, 063823 (2009).
[14] C. T. Putkunz *et al.*, Phys. Rev. Lett. **106**, 013903 (2011).
[15] K. A. Nugent, A. G. Peele, H. M. Quiney, and H. N. Chapman, Acta Crystallogr. Sect. A **61**, 373 (2005).
[16] R. Hegerl and W. Hoppe, Ber. Bunsen-Ges. Phys. Chem. **74**, 1148 (1970).
[17] P. D. Nellist, B. C. McCallum, and J. M. Rodenburg, Nature (London) **374**, 630 (1995).
[18] J. M. Rodenburg and H. M. L. Faulkner, Appl. Phys. Lett. **85**, 4795 (2004).
[19] P. Thibault *et al.*, Science **321**, 379 (2008).
[20] F. Hüe, J. M. Rodenburg, A. M. Maiden, and P. A. Midgley, Ultramicroscopy **111**, 1117 (2011).
[21] L. Bourgeois *et al.*, Cryst. Growth Des. **11**, 3141 (2011).
[22] M. Haider *et al.*, Ultramicroscopy **75**, 53 (1998).
[23] J. M. Rodenburg and A. M. Maiden (private communication).
[24] J. R. Fienup, Appl. Opt. **21**, 2758 (1982).
[25] V. Elser, J. Opt. Soc. Am. A **20**, 40 (2003).
[26] D. Shapiro *et al.*, Proc. Natl. Acad. Sci. U.S.A. **102**, 15 343 (2005).
[27] B. Abbey *et al.*, Appl. Phys. Lett. **93**, 214101 (2008).
[28] B. Abbey *et al.*, Nature Photon. **5**, 420 (2011).
[29] J. N. Clark and A. G. Peele, Appl. Phys. Lett., **99**, 154103 (2011).
[30] C. Maunders, C. Dwyer, P. C. Tiemeijer, and J. Etheridge, Ultramicroscopy **111**, 1437 (2011).